Electronic Supplementary Material (ESI) for Materials Horizons.
This journal is © The Royal Society of Chemistry 2023

Supplementary Information

Tailor-made β-ketoenamine-linked covalent organic polymer nanofilms for precise molecular sieving

Hukang Guo [a, b], Chuanjie Fang [a, b, *], Fupeng Li [a, b], Wenshou Cui [a, b], Ruiyan Xiong [a, b], Xing Yang [d], Liping Zhu [a, b, c, *]

[a] *MOE Key Laboratory of Macromolecular Synthesis and Functionalization, Department of Polymer Science and Engineering, Zhejiang University, Hangzhou 310058, P.R. China*

[b] *MOE Engineering Research Center of Membrane and Water Treatment Technology, Zhejiang University, Hangzhou 310058, P.R. China*

[c] *Center for Healthcare Materials, Shaoxing Institute, Zhejiang University, Shaoxing 312000, P.R. China*

[d] *Department of Chemical Engineering, KU Leuven, Celestijnenlaan 200F, B-3001 Heverlee, Belgium*

* Corresponding author
Dr. Fang, fangchuanjie@zju.edu.cn
Prof. Zhu, lpzhu@zju.edu.cn

1. Materials and experiments

1.1. Materials

Polyimide granules (P84) were purchased from HP Polymer GmbH (Austria). Si/SiO_2 wafer with a 300 ± 10 nm oxide layer was purchased from Lijing Keji Co., Ltd. (Zhejiang, China). Trimesoyl chloride (TMC, 98%), p-phenylenediamine (Pa, 97%), tris(4-aminophenyl)amine (TAPA, 98%), 1,6-hexanediamine (HDA, 99%) were supplied by Macklin Biochemical Co., Ltd. (Shanghai, China). 1,3,5-Triformylphloroglucinol (Tp, 97%), and benzidine (BD, 97%) were provided by Yanshen Technology Co., Ltd. (Jilin, China). 4,4'-Azodianiline (Azo, 97%) was purchased from Energy Chemical Co., Ltd. (Shanghai, China). Dimethyl formamide (DMF, 99.5%), tetrahydrofuran (THF, 99.0%), acetone (99.5%), isopropanol (99.7%), ethanol (99.7%), acetonitrile (99.0%), methanol (99.5%), hexane (98.5%), and poly(methyl methacrylate) (PMMA) were bought from Sinopharm Chemical Reagent Co., Ltd. (Shanghai, China). 3-Aminopropyltriethoxysilane (APTES, 99%), 3,3'-dimethoxybenzidine ($BD(OMe)_2$, 97%), solvent yellow 2, basic orange 2, azure B, methyl orange, sunset yellow, acid black 1, acid blue 90, rose bengal, vitamin B12 (VB12), were purchased from Aladdin Chemistry Co., Ltd. (Shanghai, China). Cefixime (99.1 %) and (Z)-2-(2-aminothiazol-4-yl)-2-((2-methoxy-2-oxoethoxy)imino)acetic acid (NICA, 97.2 %) were obtained from Bide Pharmatech Co., Ltd. (Shanghai, China). All chemicals and reagents were directly used without further treatment.

1.2. Preparation of free-standing COP nanofilms

The preparation process of the nanofilms is shown in **Fig. S3**. Silica wafers (Si/SiO_2) and quartz slides (40×40 mm^2) were first treated with hot piranha solution followed by cleaning with acetone, ethanol, and deionized water. The hydroxyl-functionalized substrates were immersed in a toluene solution of APTES (2 v%). The amino-functionalized substrates (Si/SiO_2-NH_2 and quartz-NH_2) were obtained after 100 °C heat treatment under reduced pressure and stored in ethanol.[1]

To begin with, Si/SiO_2-NH_2 substrates were washed thoroughly with THF. They were soaked in a solution of 0.3 wt% TMC in THF for 30 s, followed by rinsing with THF twice. Then they were immersed in a solution of 0.3 wt% Pa in THF for 30 s, followed by rinsing with THF twice. After drying under 60 °C for 2 min, the obtained arylamine-functionalized substrates (Si/SiO_2-Pa) were applied to grow the TpBD nanofilm. 0.2 mmol Tp (42 mg) and 0.3 mmol BD (55.3 mg) monomers were dissolved in 80 g THF containing 50 µL acetic acid, respectively. The Si/SiO_2-Pa was dipped into the Tp solution for 1 min, followed by rinsing with THF twice. Afterward, the Si/SiO_2-Pa was placed into the BD solution for 1 min and similarly rinsed with THF twice. So far, one cycle was completed. After the further completion of the desired cycles, the Si/SiO_2-Pa was dried under 60 °C for 5 min and the resultant nanofilm was named TpBD-X (X referred to the number of deposition cycles). For quartz substrates, the same procedures were implemented as described above.

The TpBD nanofilm on the wafer was transferred onto porous anodic aluminum oxide (AAO) substrate,[2] as shown in **Fig. S4**. A thin protecting layer was spin-coated on the surface of the nanofilm (8 wt% PMMA solution in chlorobenzene). Then, the substrate was etched with hydrofluoric acid (2 v%) for 2 h to float TpBD/PMMA film on the water surface. The AAO substrate was used to support the composite film at a certain dip angle underwater. Finally, the free-standing TpBD nanofilm was dried at room temperature after removing the PMMA protecting layer with acetone.

1.3. Preparation of crosslinked polyimide ultrafiltration membranes (XP84)

Crosslinked polyimide ultrafiltration membranes were prepared using a non-solvent induced phase separation (NIPS) method.[3] In brief, a casting solution was obtained by dissolving 24 wt% P84 in DMF and stirring overnight under a 60 °C water bath. After removing bubbles by centrifugation, the casting solution was then cast on the smooth side of polyester non-woven fabrics attached onto a glass plate using a casting knife with a gap of 250 μm. Then, the whole glass plate was horizontally immersed in the deionized water bath at 30 °C where the phase inversion process occurred. After 10 min, membranes were transferred into fresh water, removing residual DMF for 6 h. The obtained membranes were put into IPA for 6 h to exchange water. Afterward, they were immersed in a solution of 20 g L^{-1} 1,6-hexanediamine in IPA for 24 h at room temperature. The membranes were then taken out and washed with IPA for 3 h to remove any residual 1,6-hexanediamine. Finally, the obtained crosslinked membranes (named XP84) were stored in ethanol for subsequent substrate membranes.

1.4. Preparation of the COP TFC membranes

XP84 ultrafiltration membranes were used as porous substrates to prepare the COP TFC membranes. The XP84 surface has plenty of residual amino groups and could react with TMC and Pa for arylamine functionalization. Detailedly, the same process as the preparation of the Si/SiO_2-NH_2 substrate was employed to obtain the XP84-Pa substrate. Subsequently, the alternate deposition processes were applied to the XP84-Pa (**Fig. S3**). After being activated in DMF under 25 °C for 16 h, the membrane was exchanged with ethanol for 4 h. The residual monomers and formed oligomers in the membrane pores were removed by DMF. Finally, the as-prepared TFC membrane was soaked in ethanol for subsequent performance tests and denoted as TpBD-X (X referred to the number of deposition cycles) TFC membrane. The control group XP84 which was treated by TMC and Pa and activated by DMF was denoted as XP84-Pa. The same process was applied to other amine precursors (Pa, TAPA, $BD(OMe)_2$, and Azo) for preparing the corresponding COP TFC membranes (**Fig. S1**).

1.5. Synthesis of COP powders

COP powders were synthesized under the same conditions as the nanofilm preparation. 0.3 mmol BD and 0.2 mmol Tp monomers were reacted in THF under magnetic stirring at room temperature for 1 day. Similarly, other amine monomers Pa, TAPA, BD(OMe)$_2$, and Azo also reacted with Tp, respectively. The powders were collected by vacuum filtration, washed three times with THF, and dried for 12 h at 60 °C. The resultant powders were designated as TpBD, TpPa, TpTAPA, TpBD(OMe)$_2$, and TpAzo, respectively.

1.6. Characterizations

The water contact angle measurements were performed with a water contact analyzer (OCA-20, DataPhysics Instruments, Germany) at room temperature using a sessile drop method. The surface and cross-section morphologies of the COP nanofilms on different substrates were characterized with scanning electron microscopy (SEM, Hitachi SU−8010, Japan). For cross-section observing, the free-standing nanofilms on AAO substrates were fractured at room temperature and the COP TFC membranes were fractured in liquid nitrogen. For transmission electron microscopy (TEM, Hitachi HT−7700, Japan) imaging, the composite membranes peeled off PET non-woven fabrics were embedded in the epoxy resin and cut into *ca.* 80 nm slices at room temperature using an ultramicrotome (EMUC7, Leica, Germany). The surface topography and thickness of membranes were obtained by atomic force microscopy (AFM, Veeco MultiMode, USA) under tapping mode at a rate of 1.0 Hz. The Si/SiO$_2$ substrates covered with the nanofilms were scratched to expose the bottom surface using a sharp scalpel. The thickness of nanofilms deposited on Si/SiO$_2$ substrates was monitored by a spectroscopic ellipsometer (UVISEL, Horiba, France) at an incidence angle of 70° within the range of 0.6−5 eV.

The UV-vis absorption spectra of the TpBD nanofilms on quartz substrates were detected by a UV-vis spectrophotometer (UV−2600, Shimadzu, Japan) with a wavelength range of 200 to 800 nm. A nano-infrared spectrometer (nano-IR, nanoIR2-fs, Anasys Instruments, USA) was applied to characterize the surface chemical composition and morphology of the TpBD nanofilm under contact mode. The surface chemistry properties of COP TFC membranes were also analyzed by an attenuated total reflectance Fourier transform infrared spectrometer (ATR−FTIR, Thermo Fisher Nicolet 6700, USA) and an X-ray photoelectron spectroscopy (XPS, Thermo ESCALAB 250XI, USA). A Fourier transform infrared spectrometer (FTIR, Bruker Vector-22, Germany) was employed to analyze the chemical compositions of COP powders. The crystalline property of COP powders was probed using a powder X-ray diffractometer (PXRD, X'Pert3 Powder, Holland) with a Cu Kα radiation source (λ = 1.54056 Å) at a scan step size of 0.026°. A surface area and porosity analyzer instrument (Quantachrome Autosorb IQ3, USA) was used to record CO_2 sorption isotherms of COP powders at 273 K.

1.7. Membrane performance measurements

The permeation and rejection performance of the COP TFC membranes were evaluated by a dead-end stirred cell (Millipore Co., USA) with an effective area of 12.5

cm^2. All tests were finished at 25 °C. Each membrane was exchanged with the selected solvent for 0.5 h before a test. To get stable permeance, the membrane was pre-pressured in the device under 4 bar for 0.5 h. Afterward, the permeate volume was recorded under the target pressure. In this work, different organic solvents (acetonitrile, methanol, acetone, ethanol, isopropanol, and hexane) were used to evaluate membrane permeance (P, L m^{-2} h^{-1} bar^{-1}) calculated by Eq. (2):

$$P = \frac{V}{A \cdot \Delta t \cdot p} \tag{1}$$

where V is the solvent permeation volume (L) during the testing time Δt (h), A is the effective membrane area (m^2), and p is the applied operating pressure (bar).

A series of probe molecules with different molecular weights (solvent yellow 2, basic orange 2, azure B, methyl orange, sunset yellow, acid black 1, acid blue 90, rose bengal, and VB12) were adopted to evaluate the membrane rejection performance. Their detailed information is listed in **Table S1**. The measurements were achieved using the same device as above. The solute concentration in ethanol was fixed at 20 ppm. After one test, the membrane was cleaned with ethanol in the device for 12 h to remove residual probe molecules. The feed and permeate solutions of 5 mL were collected and their UV-vis absorption spectra were obtained by a UV–vis spectrophotometer. The rejection (R, %) was calculated using Eq. (2):

$$R = \left(1 - \frac{C_p}{C_f}\right) \times 100\% \tag{2}$$

where Cf and Cp are the concentrations of feed and permeate solutions, respectively. The concentration corresponds to the absorbance at characteristic absorption wavelength. Similarly, the molecular separation performance was probed with a mixed solution (10 ppm for one molecule). Each reported solvent permeance and rejection values were an average value determined by three membrane samples under parallel tests.

Furthermore, two APIs (NICA and cefixime, 50 ppm) dissolved in methanol were assigned to investigate practical separation performance. The rejection and separation results were detected by a UV-vis spectrophotometer and high-performance liquid chromatography (HPLC, Agilent 1260, USA). The long-term operation stability of the membrane was evaluated by a 24 h continuous filtration under 4 bar. The permeance and rejection values were recorded in a certain interval.

2. Figures

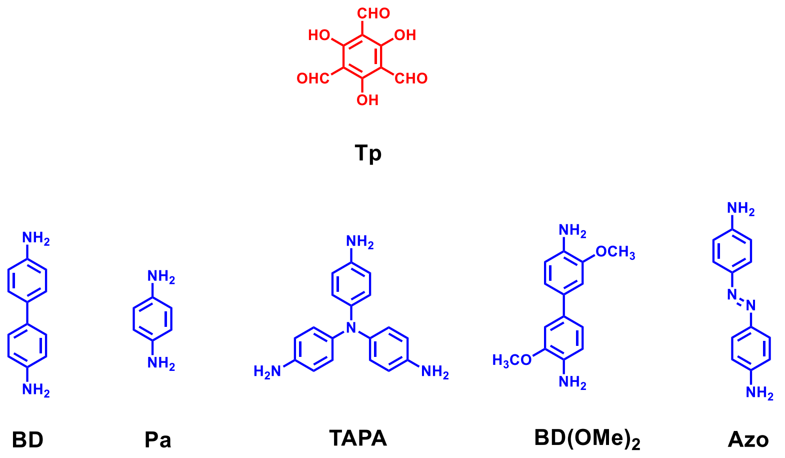

Fig. S1. Chemical structures of the aldehyde precursor and different amine precursors.

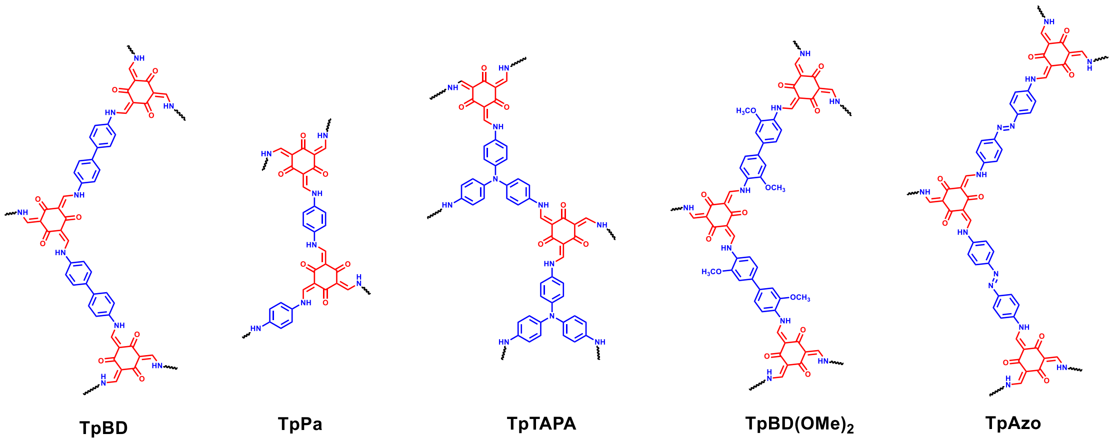

Fig. S2. Structural linkages of the TpBD, TpPa, TpTAPA, TpBD(OMe)$_2$, and TpAzo.

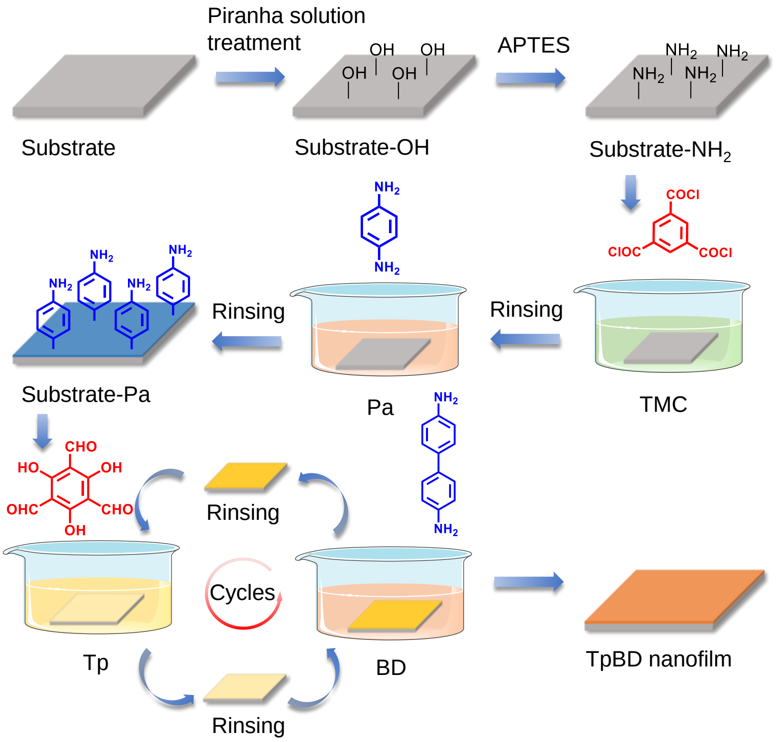

Fig. S3. Schematic illustration of the preparation process of the TpBD nanofilm on the arylamine functionalized substrate.

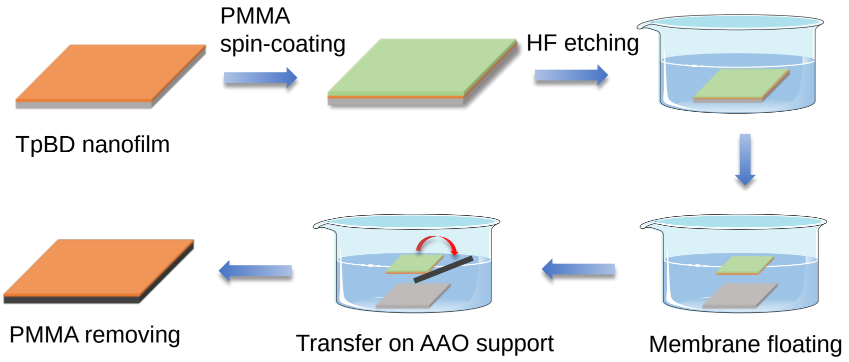

Fig. S4. Schematic illustration of the transfer process of the TpBD nanofilm.

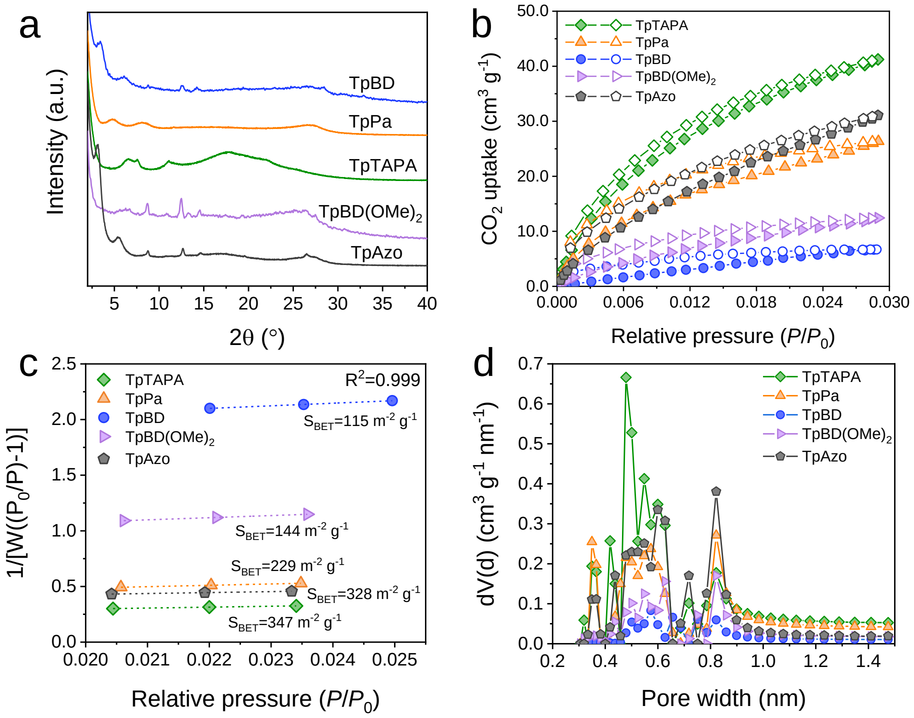

Fig. S5. Crystalline and microporous characteristics of different COP powders synthesized in the solvent of THF. (a) PXRD patterns. (b) CO_2 sorption isotherms measured at 273 K. (c) BET plots calculated from CO_2 adsorption isotherms. (d) Pore size distributions calculated by fitting the NLDFT model to the adsorption data.

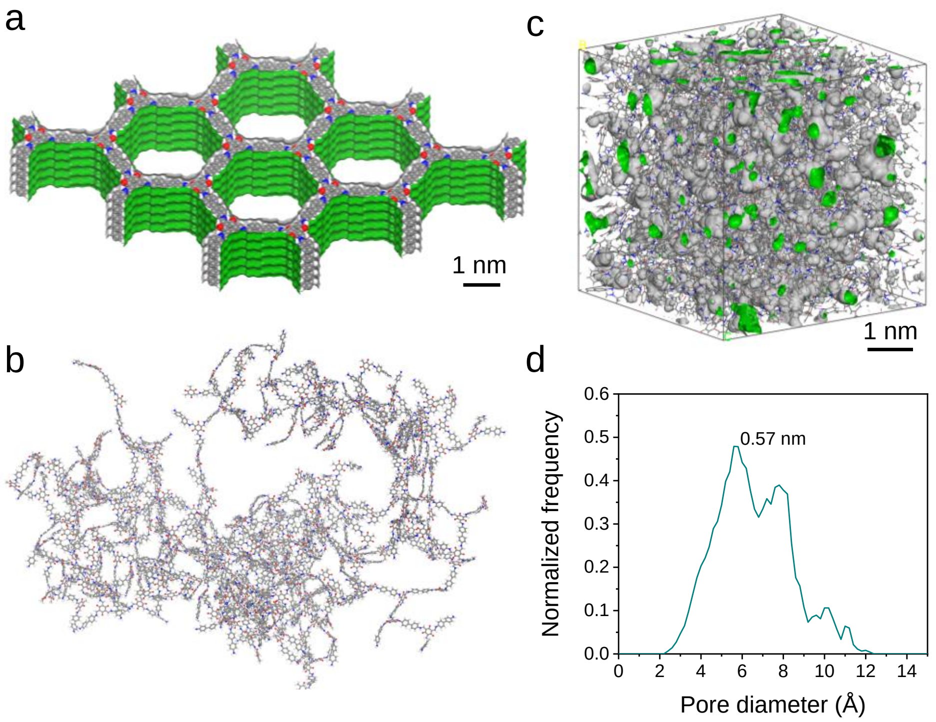

Fig. S6. (a) Three-dimensional view of highly-ordered TpBD segments based on the AA stacking mode. (b) Structural representation of randomly connected TpBD crosslinked networks. (c) Three-dimensional view of an amorphous cell of the TpBD polymer. The grey surface indicates the van der Waals surface, and the green surface is the Connolly surface with a probe radius of 1.55 Å, representing the accessible free volume. (d) Pore size distribution calculated by the simulated amorphous cell of the TpBD.

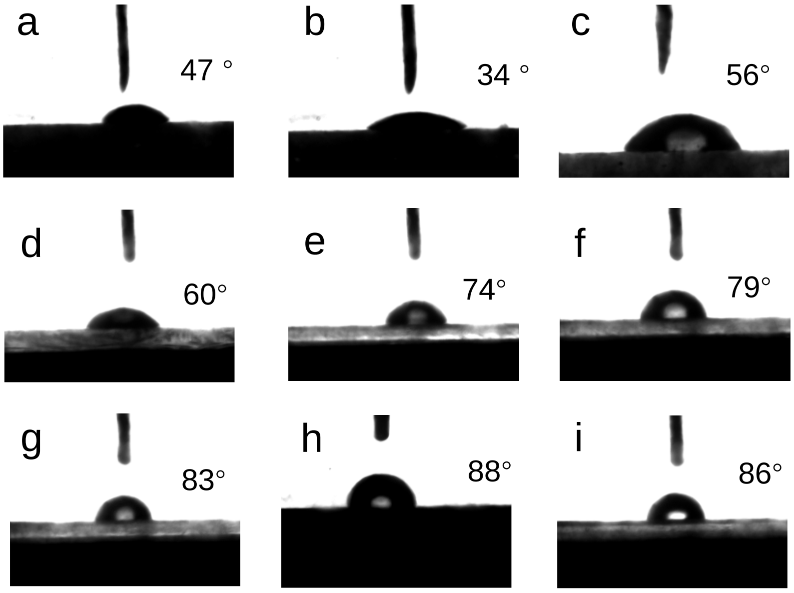

Fig. S8. Digital photographs of water contact angles (WCAs) of the quartz (a), quartz-OH (b), quartz-NH_2 (c), and quartz-Pa (d) substrates and TpBD-3 (e), TpBD-5 (f), TpBD-7 (g), TpBD-10 (h), and TpBD-15 (i) nanofilms.

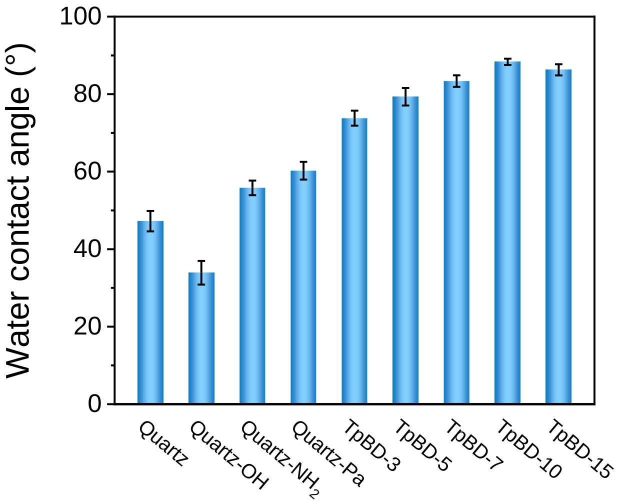

Fig. S9. WCAs of quartz substrates through different surface modifications and the TpBD nanofilms with different deposition numbers.

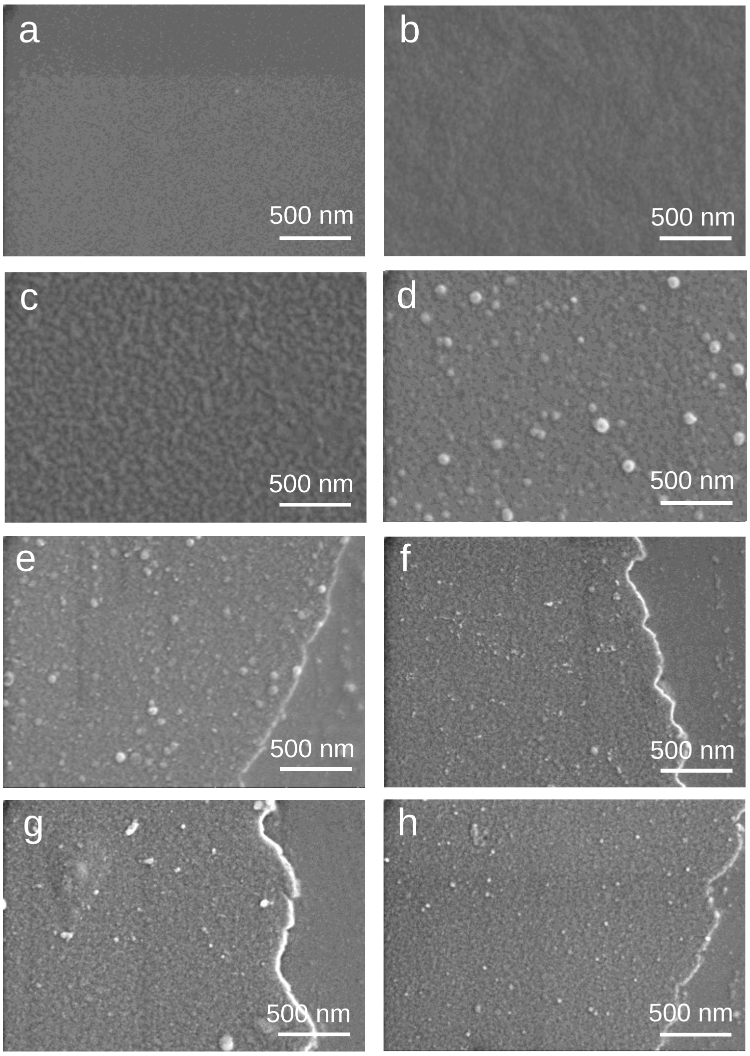

Fig. S10. Surface SEM images of the Si/SiO_2 (a), Si/SiO_2-NH_2 (b), and Si/SiO_2-Pa (c) substrates and TpBD-3 (d), TpBD-5 (e), TpBD-7 (f), TpBD-10 (g), and TpBD-15 (h) nanofilms.

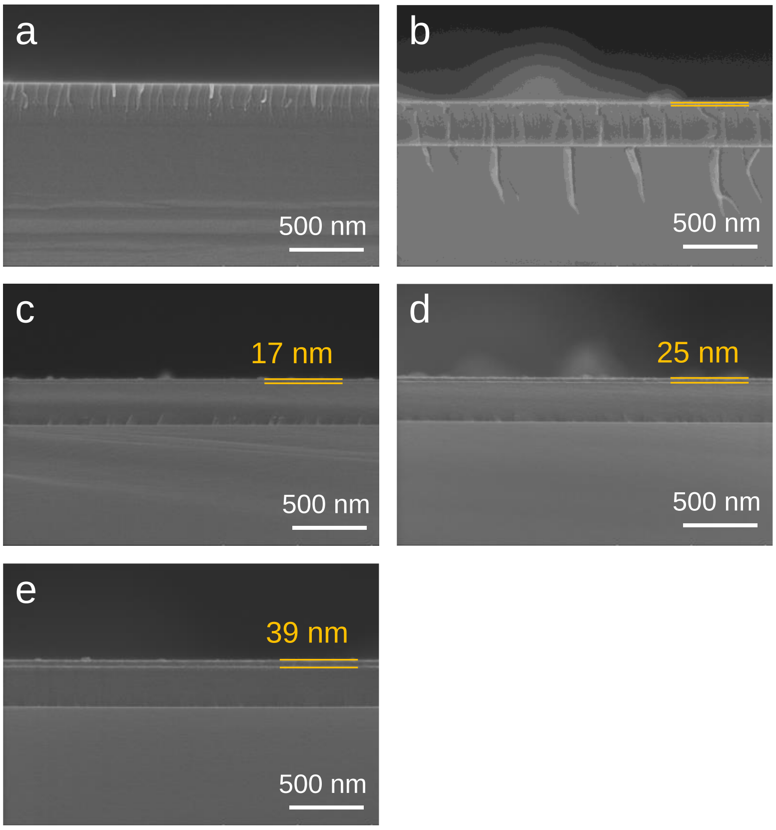

Fig. S11. Cross-section SEM images of the Si/SiO$_2$ substrate (a) and TpBD-5 (b), TpBD-7 (c), TpBD-10 (d), and TpBD-15 (e) nanofilms.

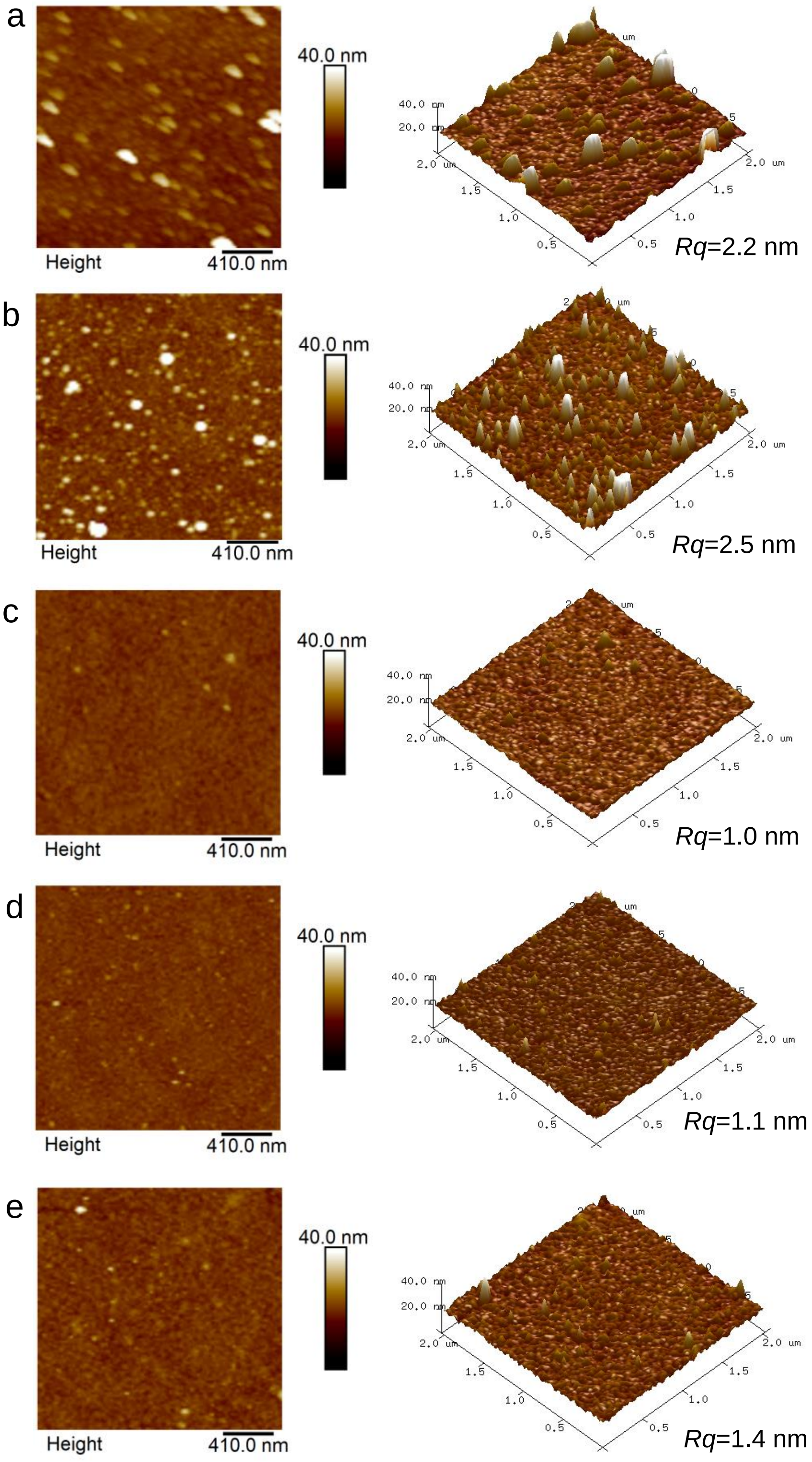

Fig. S12. AFM images of the TpBD-3 (a), TpBD-5 (b), TpBD-7 (c), TpBD-10 (d), and TpBD-15 (e) nanofilms.

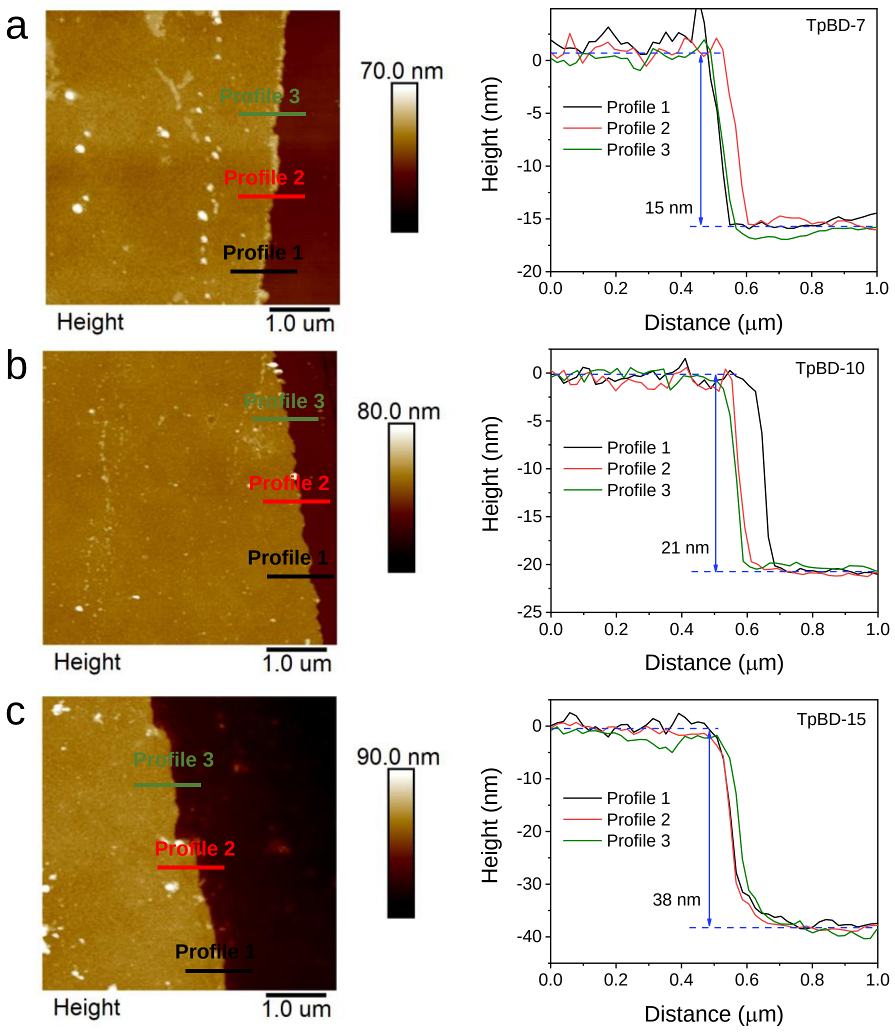

Fig. S13. AFM images and corresponding height profiles of the TpBD-7 (a), TpBD-10 (b), and TpBD-15 (c) nanofilms on top of Si/SiO$_2$ substrates.

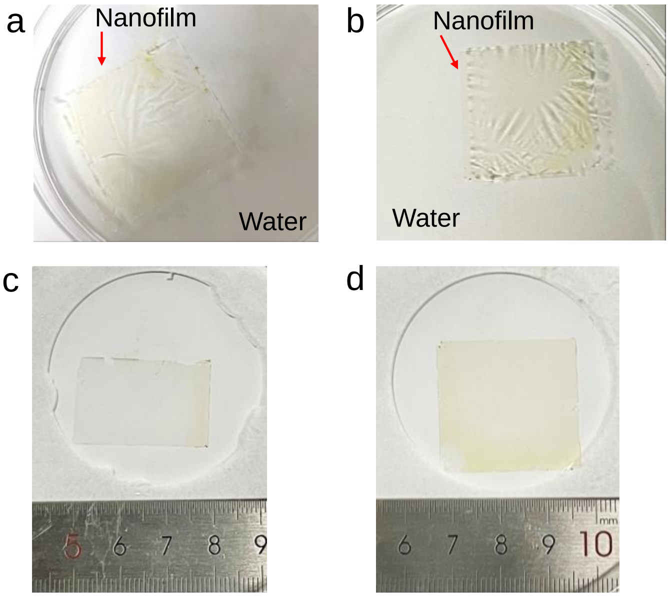

Fig. S14. Photographs of free-standing TpBD-10 (a, c) and TpBD-15 (b, d) nanofilms with PMMA protect layers floated on the water surface and transferred to AAO substrates, respectively.

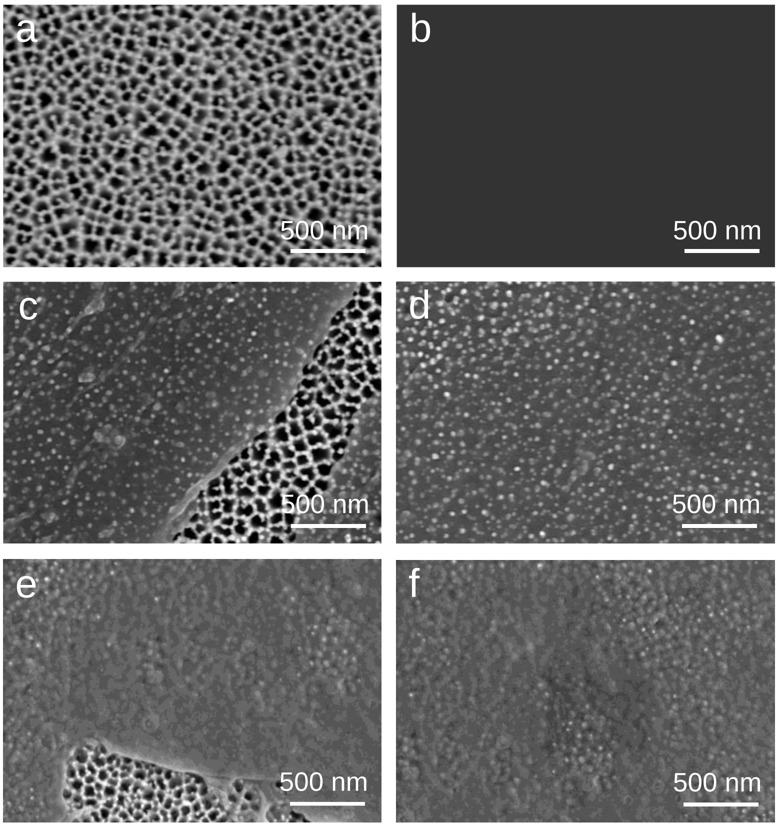

Fig. S15. Surface SEM images of the AAO substrate (a), PMMA protecting layer (b), TpBD-10 nanofilm (c, d), and TpBD-15 nanofilm (e, f).

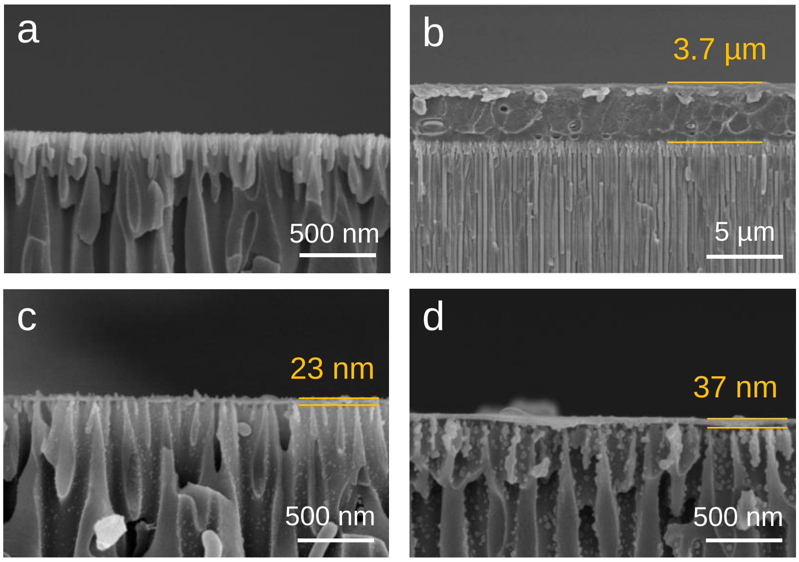

Fig. S16. Cross-section SEM images of the AAO substrate (a), PMMA protecting layer (b), TpBD-10 nanofilm (c), and TpBD-15 nanofilm (d).

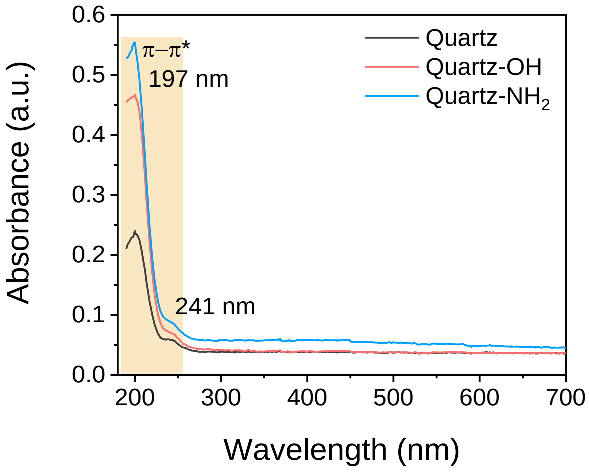

Fig. S17. UV absorption spectra of quartz substrates after surface modifications.

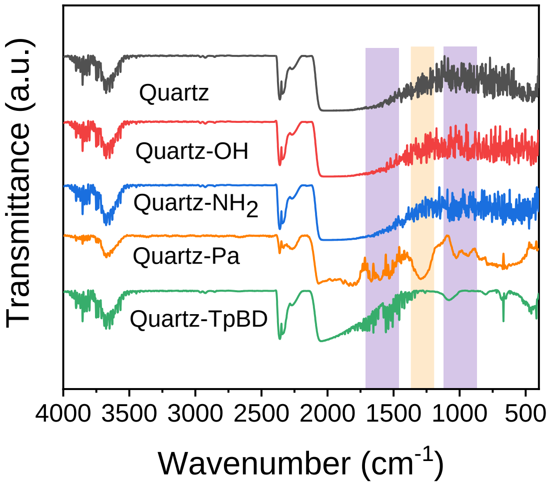

Fig. S18. FTIR spectra of quartz slides after surface modifications and covered the TpBD-15 nanofilm.

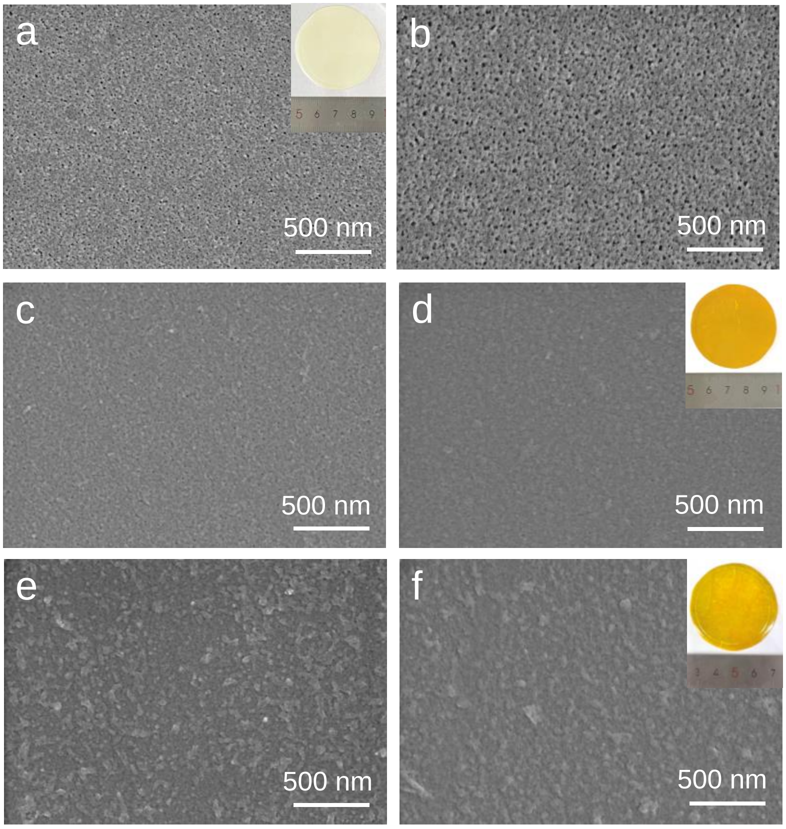

Fig. S19. Surface SEM images of the XP84 (a), XP84-Pa (b), and the corresponding TpBD-3 (c), TpBD-5 (d), TpBD-7 (e), and TpBD-10 (f) TFC membranes. Insets: digital photographs of the membranes.

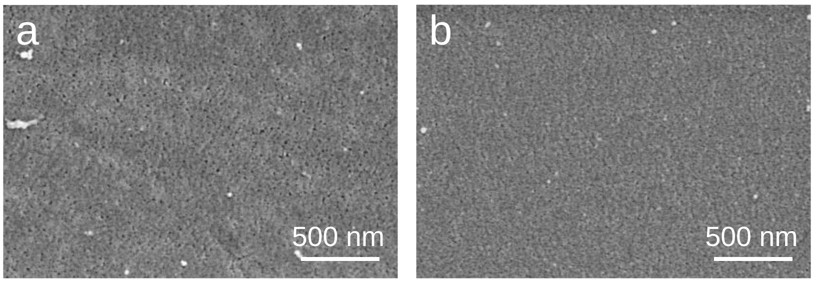

Fig. S20. Surface SEM images of the XP84 substrates treated by a solvent of THF (a) and DMF (b).

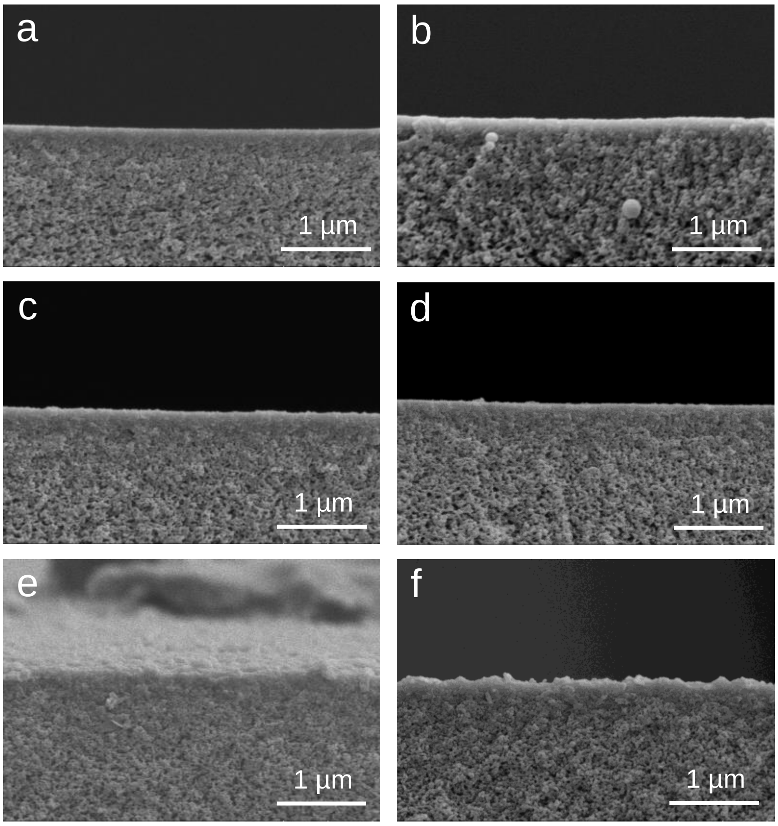

Fig. S21. Cross-section SEM images of the XP84 (a), XP84-Pa (b), and the corresponding TpBD-3 (c), TpBD-5 (d), TpBD-7 (e), and TpBD-10 (f) TFC membranes.

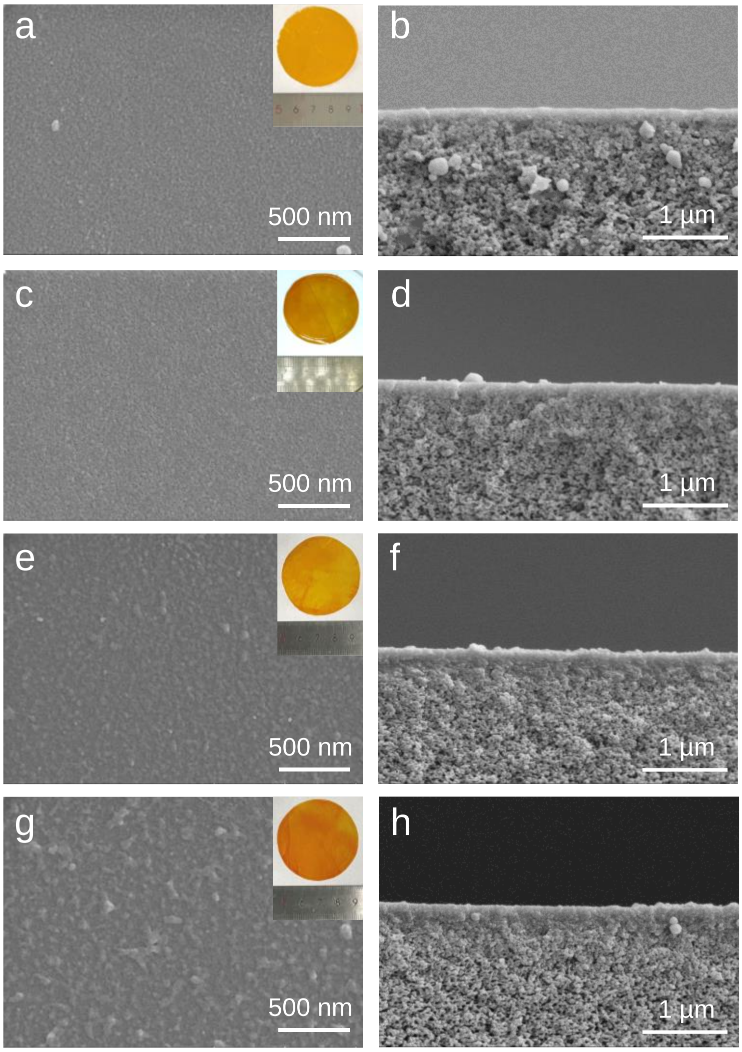

Fig. S22. Surface and cross-section SEM images of the TpPa-5 (a, b), TpTAPA-5 (c, d), TpBD(OMe)$_2$-10 (e, f), and TpAzo-10 (g, h) TFC membranes. Insets: digital photographs of the TFC membranes.

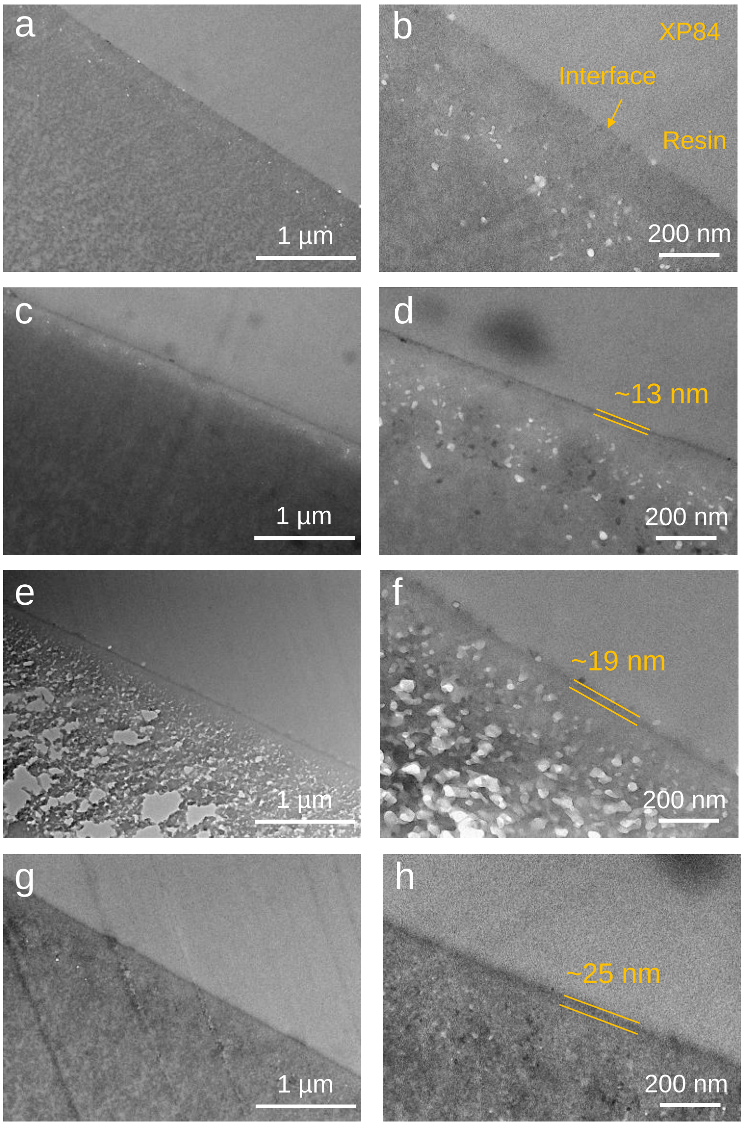

Fig. S23. Cross-section TEM images of the XP84 (a, b) and TpBD-5 (c, d), TpBD-7 (e, f), and TpBD-10 (g, h) TFC membranes.

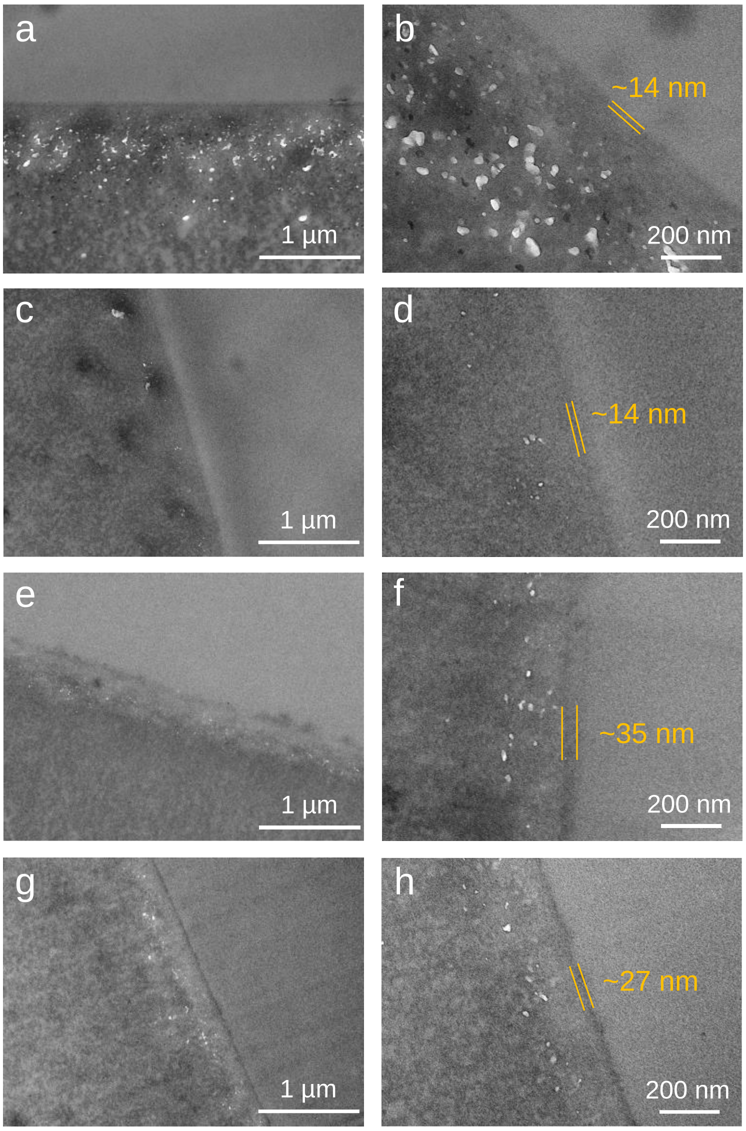

Fig. S24. Cross-section TEM images of the TpPa-5 (a, b), TpTAPA-5 (c, d), TpBD(OMe)$_2$-10 (e, f), and TpAzo-10 (g, h) TFC membranes.

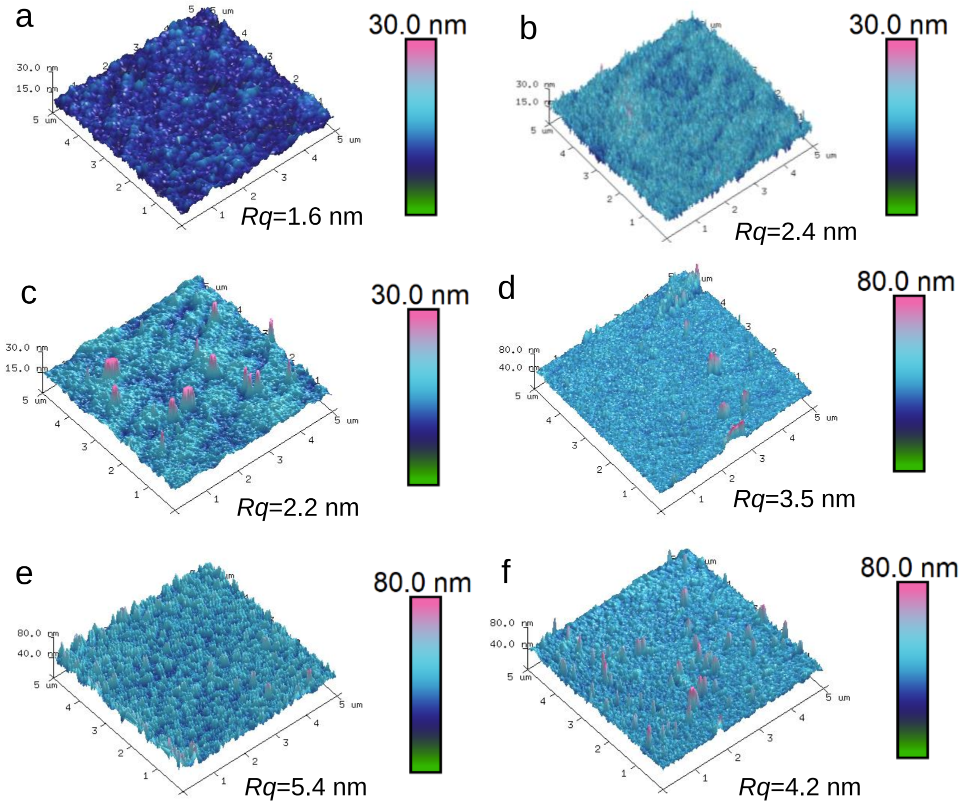

Fig. S25. AFM images of the XP84 (a), XP84-Pa (b), and the corresponding TpBD-3 (c), TpBD-5 (d), TpBD-7 (e), and TpBD-10 (f) TFC membranes.

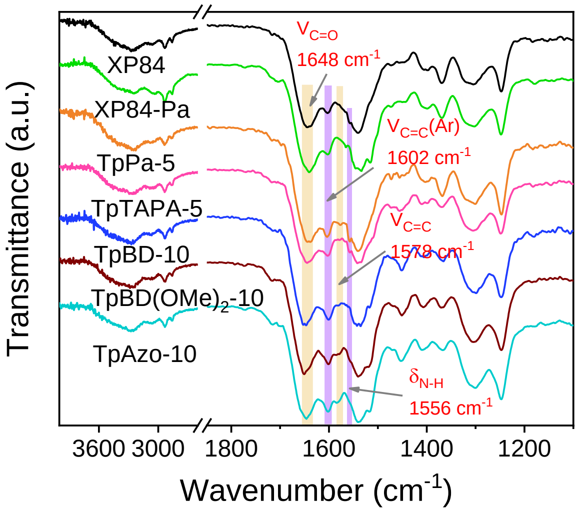

Fig. S26. ATR-FTIR spectra of different COP TFC membranes.

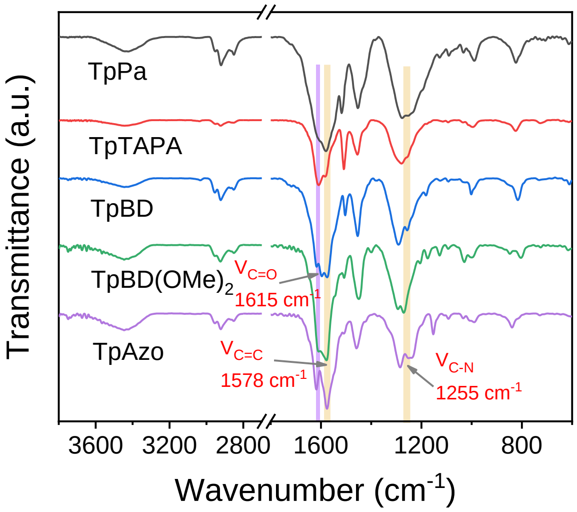

Fig. S27. FTIR spectra of different COP powders.

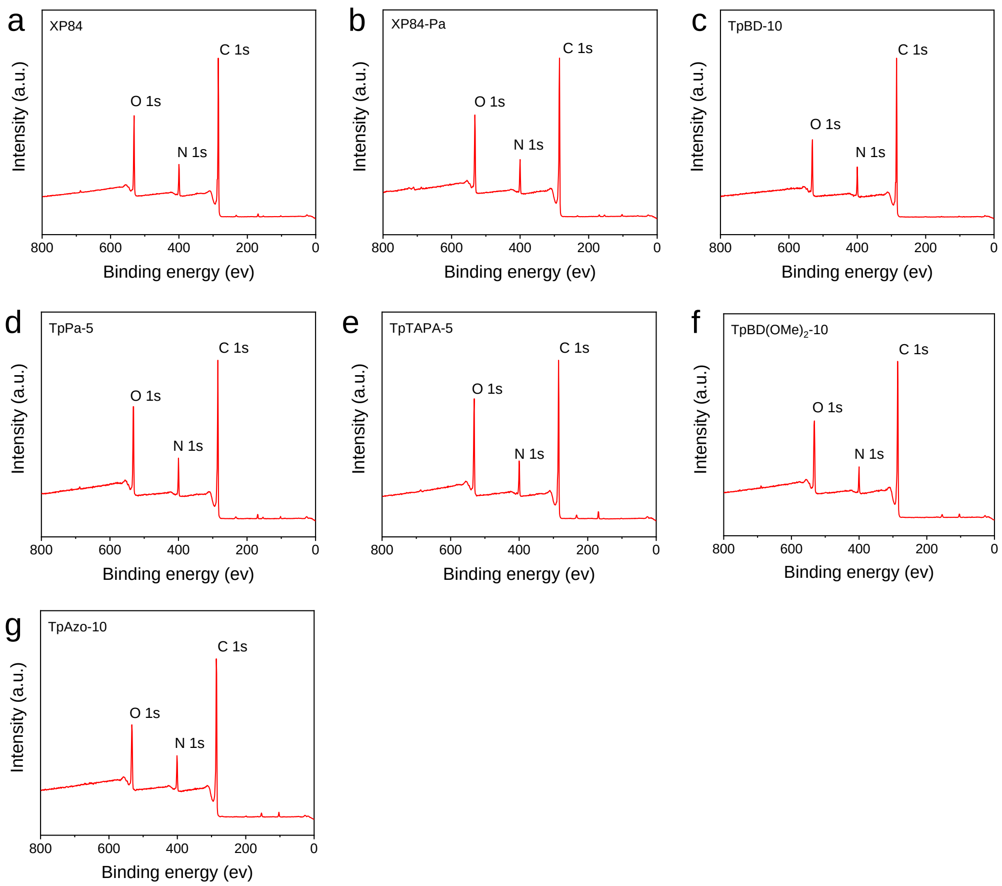

Fig. S28. XPS survey spectra of different COP TFC membranes.

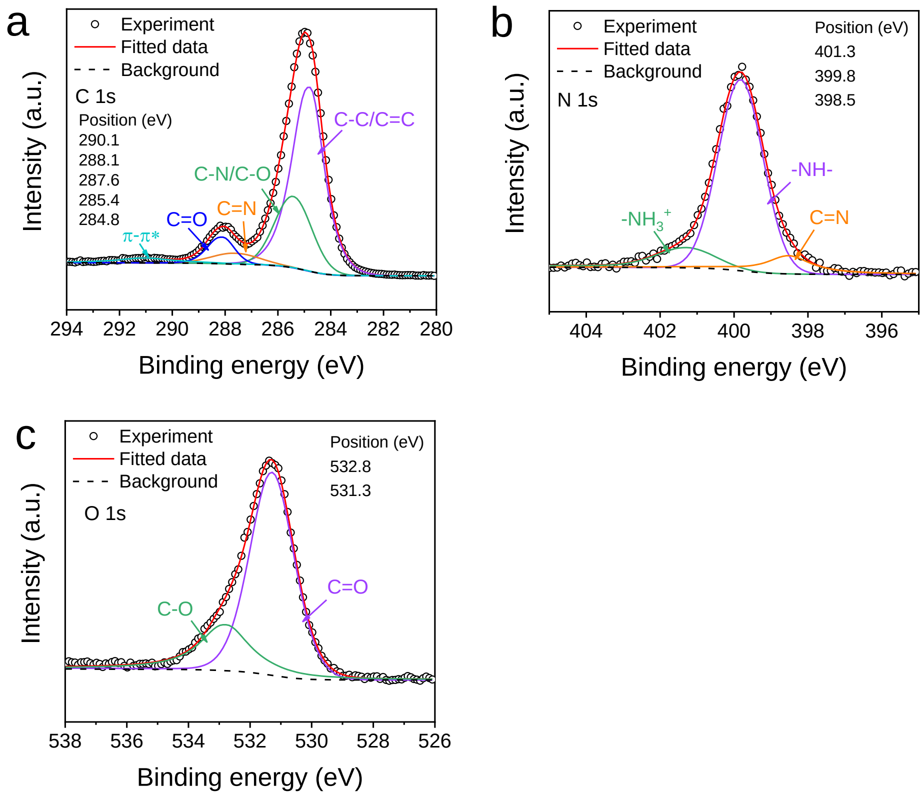

Fig. S29. High-resolution XPS spectra of C 1s (a), N 1s (b), and O 1s (c) of the TpBD-10 TFC membrane.

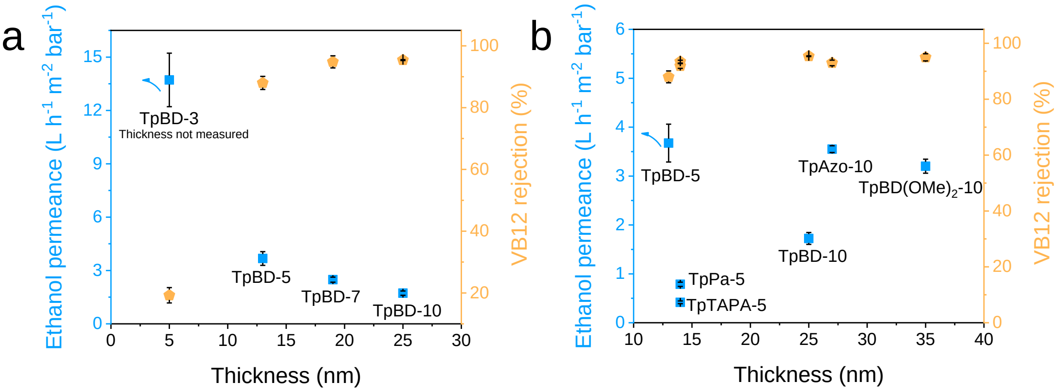

Fig. S30. (a) The relationship between the thickness of TpBD nanofilms and OSN performance. (b) The relationship between the thickness of different COP nanofilms and OSN performance.

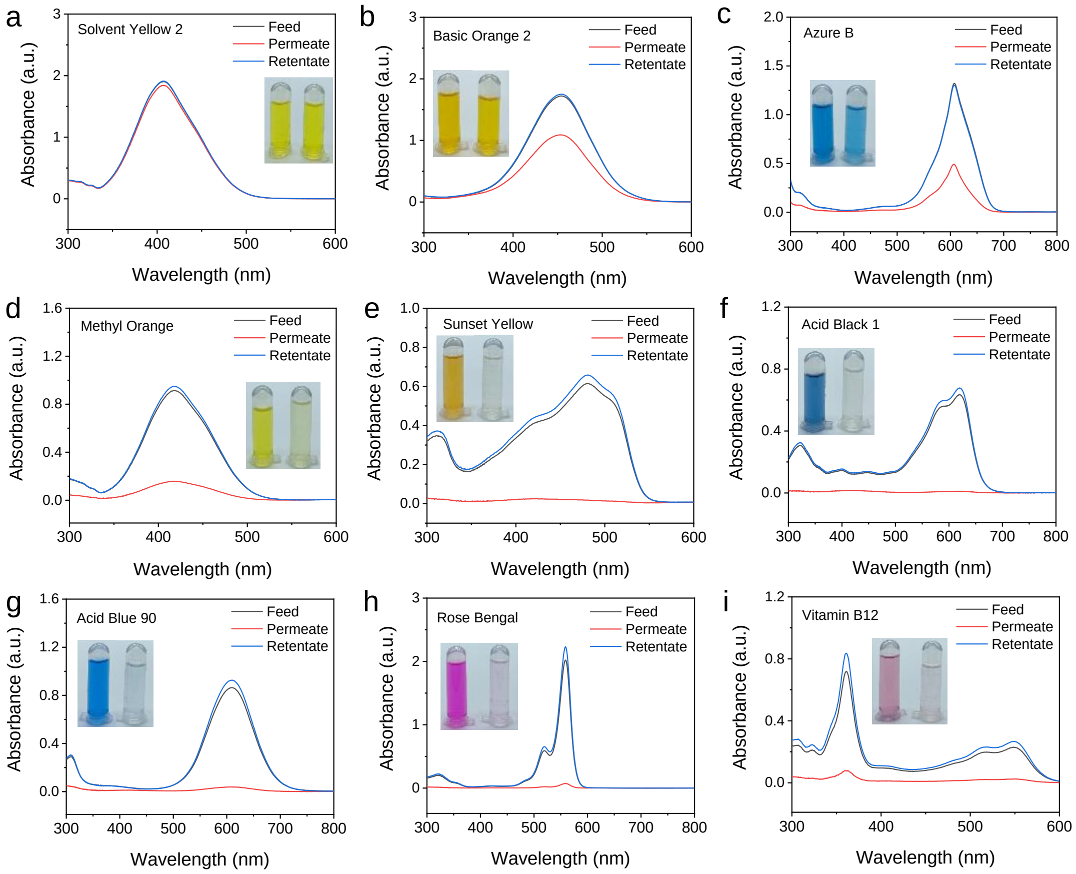

Fig. S31. UV absorption spectra of various ethanolic solutions of solute molecules before and after filtration through the TpBD-5 TFC membrane. Insets: digital photographs of feed (left) and permeate (right) solutions.

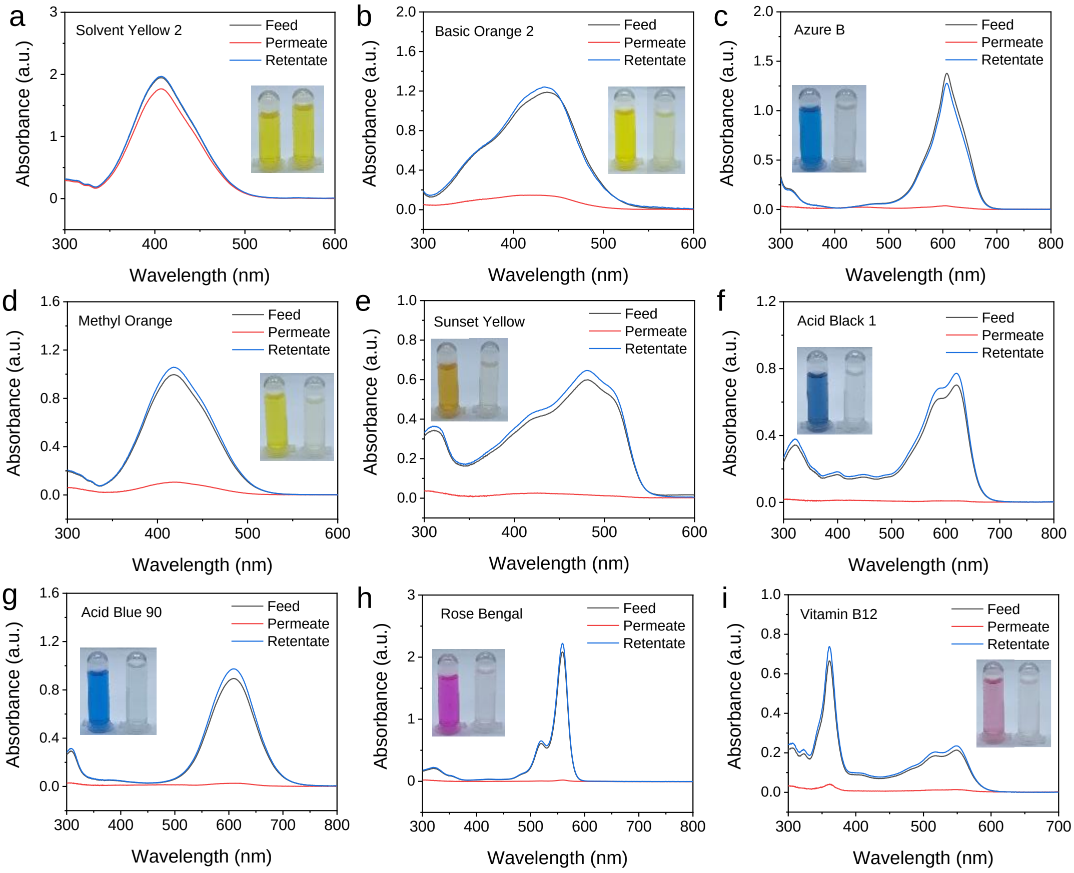

Fig. S32. UV absorption spectra of various ethanolic solutions of solute molecules before and after filtration through the TpBD-10 TFC membrane. Insets: digital photographs of feed (left) and permeate (right) solutions.

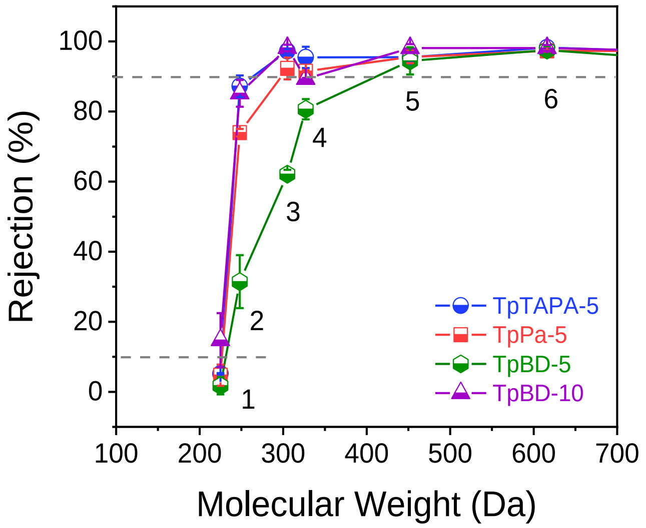

Fig. S33. The enlarged plot of rejection performance toward various molecules in ethanol (20 ppm) under 4 bar.

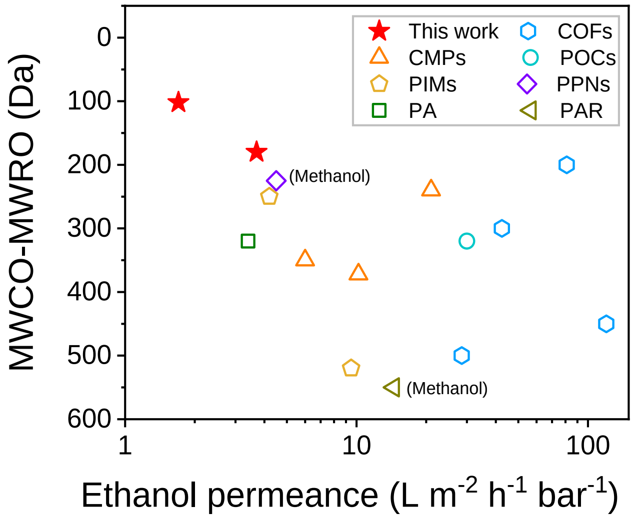

Fig. S34. Comparison of permeance and rejection accuracy between our membranes and other reported membranes in references. The detailed data are listed in **Table S4**.

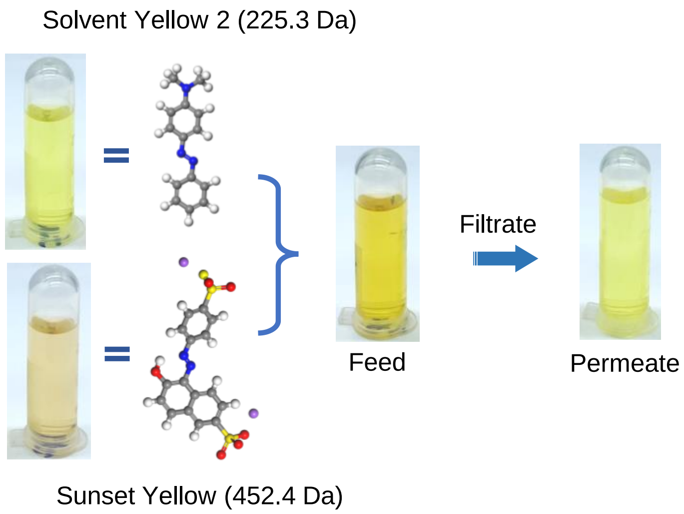

Fig. S35. Digital photographs of the mixed ethanolic solutions of solvent yellow 2 and sunset yellow molecules before and after filtration through the TpBD-10 TFC membrane.

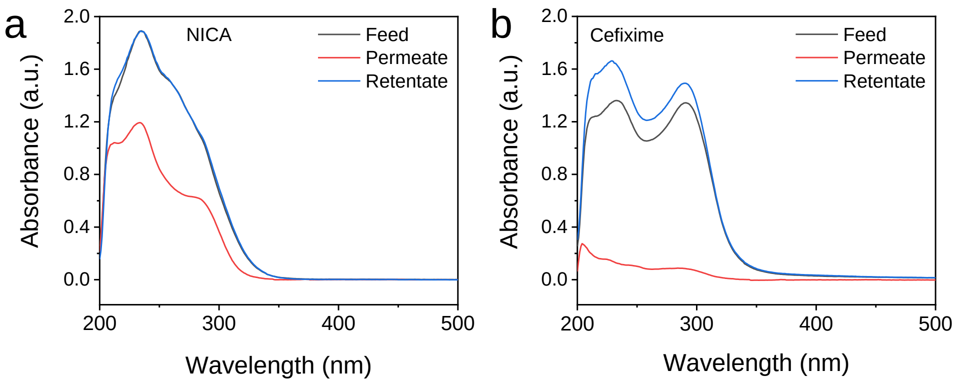

Fig. S36. UV absorption spectra of NICA and cefixime methanol solutions (50 ppm) before and after filtration through the TpBD-10 TFC membrane.

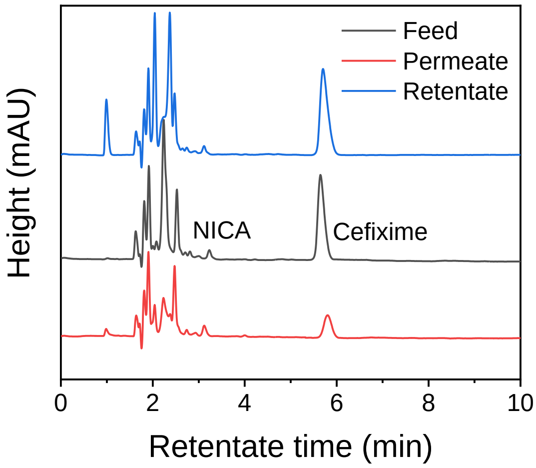

Fig. S37. HPLC chromatograms of the separated NICA and cefixime through the TpBD-10 TFC membrane.

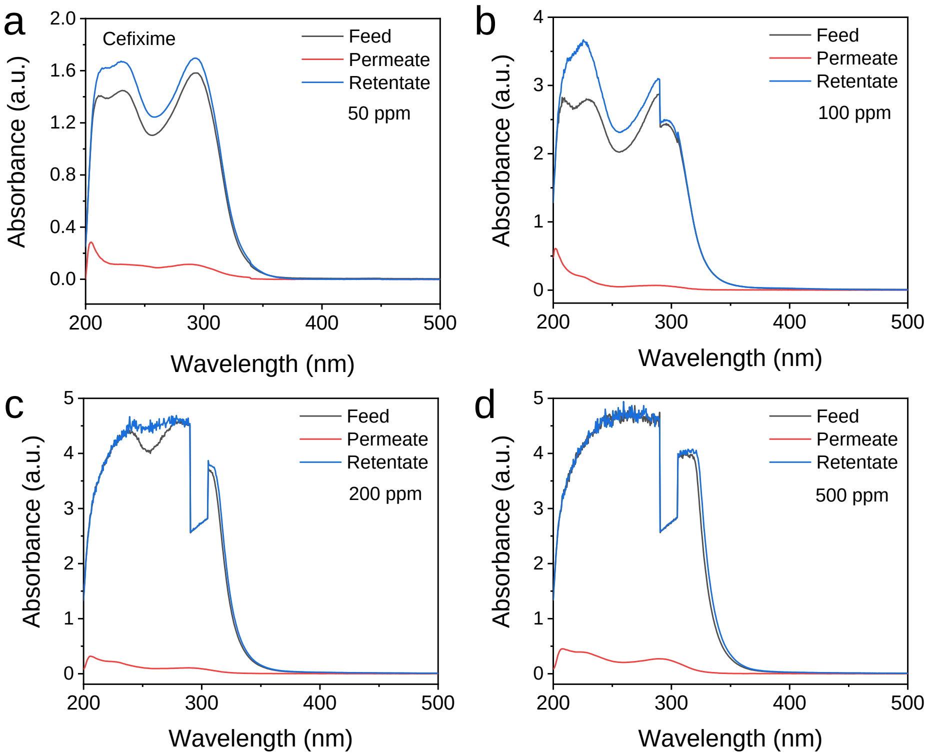

Fig. S38. UV absorption spectra of the feed, permeate, and retentate solutions when filtrating the methanolic cefixime solutions with a concentration of 50 (a), 100 (b), 200 (c), 500 (d) ppm through the TpBD-10 TFC membrane.

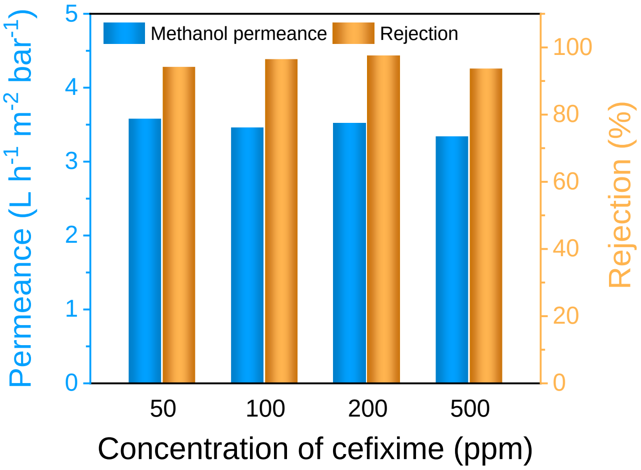

Fig. S39. Permeance and rejection while filtrating the methanolic cefixime solutions with various concentrations through the TpBD-10 TFC membrane under 4 bar.

3. Tables

Table S1. Detailed properties of different solute molecules used in this work.

Solutes	Molecular weight (g/mol)	Charge	Characteristic absorption peak (nm)
Solvent Yellow 2	225.29	0	408
Basic Orange 2	248.71	+1	449
Azure B	305.83	+1	608
Methyl Orange	327.33	−1	420
Sunset Yellow	452.36	−2	482
Acid Black 1	616.49	−2	618
Acid Blue 90	854.02	−1	610
Rose Bengal	1017.64	−2	558
Vitamin B12	1355.38	0	362

Table S2. Element compositions of different COP TFC membranes.

Membranes	C (%)	N (%)	O (%)
XP84	74.6	10.1	15.3
XP84-Pa	74.7	9.8	15.5
TpBD-10	77.6	9.6	12.7
TpPa-5	72.0	9.9	18.1
TpTAPA-5	71.0	10.5	18.2
TpBD(OMe)$_2$-10	75.6	7.2	17.2

TpAzo-10	75.5	10.2	14.4

Table S3. Solvent properties and corresponding calculated $\frac{\delta_p}{\eta d_m^2}$ values.

Solvent	d_m [a] (×10^{-9}, m)	η [b] (×10^{-3}, Pa s)	δ_p [c] (×10^{3}, $\mathrm{Pa}^{0.5}$)	$\frac{\delta_p}{\eta d_\mathrm{m}^2}$ (×10^{24}, $\mathrm{Pa}^{-0.5}$ s^{-1} m^{-2})
Hexane	0.75	0.29	0	0
Isopropanol	0.62	2.06	6.1	7.71
Ethanol	0.57	1.08	8.8	25.06
Acetone	0.62	0.32	10.4	85.62
Methanol	0.51	0.54	12.3	87.74
Acetonitrile	0.55	0.34	18	173.99

[a] Molar diameter (d_m)

[b] Viscosity at 25 °C (η)

[c] Solubility parameter due to dipole forces (δ_p)

The data was from ref. [4-8]

Table S4. Detailed comparative data about our membranes and other OSN membranes reported in the literatures.

Membrane type	Membrane material	MWCO (Da)	MWRO (Da)	MWRO−MWCO (Da)	Ethanol permeance (L m^{-1} h^{-1} bar^{-1})	Reference
COPs	TpBD-5	410	230	180	3.7	This work
	TpBD-10	327	225	102	1.7	This work
	TpPa-5	305	225	80	0.8	This work
	TpTAPA-5	265	225	40	0.4	This work
COFs	$DP_{2h}COM$	800	600	200	81.0	9
	TpPa-Py	700	250	450	120	10
	TPF-DNF	800	300	500	28.5	11
	TFP-DHF M20	900	600	300	42.5	12
CMPs	CNT-EP-PC15	540	300	240	21.0	13
	p-CMP	560	188	372	10.2	14
	TTB-CMPO	500	150	350	6.0	15
POCs	CC3α-PAN	1370	1050	320	30	16
PIMs	AOPIM-1	800	280	520	9.48	17
	PIM-1/COF-COOH TFN	450	200	250	4.2	18
PPNs	p-PPN	600	375	225	4.5 (Methanol)	19
PA	γ-CD/TMC	550	230	320	3.4	20
PAR	PAR@mBHPF	750	200	550	14.5 (Methanol)	21

4. References

1. M. Byeon, E. Lee and J.-W. Park, *Macromolecules*, 2017, **50**, 6796-6803.
2. K. S. Kim, Y. Zhao, H. Jang, S. Y. Lee, J. M. Kim, K. S. Kim, J. H. Ahn, P. Kim, J. Y. Choi and B. H. Hong, *Nature*, 2009, **457**, 706-710.
3. M. F. Jimenez-Solomon, Q. Song, K. E. Jelfs, M. Munoz-Ibanez and A. G. Livingston, *Nat. Mater.*, 2016, **15**, 760-767.
4. S. Karan, Z. Jiang and A. G. Livingston, *Science*, 2015, **348**, 1347-1351.
5. A. Buekenhoudt, F. Bisignano, G. De Luca, P. Vandezande, M. Wouters and K. Verhulst, *J. Membr. Sci.*, 2013, **439**, 36-47.
6. C. Andecochea Saiz, S. Darvishmanesh, A. Buekenhoudt and B. Van der Bruggen, *J. Membr. Sci.*, 2018, **546**, 120-127.
7. B. Van der Bruggen, J. Schaep, D. Wilms and C. Vandecasteele, *J. Membr. Sci.*, 1999, **156**, 29-41.
8. C. Cheng, S. A. Iyengar and R. Karnik, *Nat. Nanotechnol.*, 2021, **16**, 989-995.
9. J. Yuan, X. You, N. A. Khan, R. Li, R. Zhang, J. Shen, L. Cao, M. Long, Y. Liu, Z. Xu, H. Wu and Z. Jiang, *Nat. Commun.*, 2022, **13**, 3826.
10. R. Shevate and D. L. Shaffer, *ACS Nano*, 2022, **16**, 2407-2418.
11. D. B. Shinde, L. Cao, A. D. D. Wonanke, X. Li, S. Kumar, X. W. Liu, M. N. Hedhili, A. H. Emwas, M. Addicoat, K. W. Huang and Z. P. Lai, *Chemical Science*, 2020, **11**, 5434-5440.
12. D. B. Shinde, G. Sheng, X. Li, M. Ostwal, A. H. Emwas, K. W. Huang and Z. Lai, *J. Am. Chem. Soc.*, 2018, **140**, 14342-14349.
13. Z. Y. Zhou, X. Li, D. Guo, D. B. Shinde, D. W. Lu, L. Chen, X. W. Liu, L. Cao, A. M. Aboalsaud, Y. X. Hu and Z. P. Lai, *Nat. Commun.*, 2020, **11**, 5323.
14. B. Liang, H. Wang, X. Shi, B. Shen, X. He, Z. A. Ghazi, N. A. Khan, H. Sin, A. M. Khattak, L. Li and Z. Tang, *Nat. Chem.*, 2018, **10**, 961-967.
15. X. He, H. Sin, B. Liang, Z. A. Ghazi, A. M. Khattak, N. A. Khan, H. R. Alanagh, L. S. Li, X. Q. Lu and Z. Y. Tang, *Adv. Funct. Mater.*, 2019, **29**, 900134.
16. A. He, Z. Jiang, Y. Wu, H. Hussain, J. Rawle, M. E. Briggs, M. A. Little, A. G. Livingston and A. I. Cooper, *Nat. Mater.*, 2022, **21**, 463-470.
17. Y. Jin, Q. Song, N. Xie, W. Zheng, J. Wang, J. Zhu and Y. Zhang, *J. Membr. Sci.*, 2021, **632**, 119375.
18. H. Guo, X. Xu, J. Li, W. Feng, M. Zhang, C. Fang and L. Zhu, *J. Membr. Sci.*, 2022, **660**, 120877.
19. C. X. Wang, C. X. Li, E. R. C. Rutledge, S. Che, J. Lee, A. J. Kalin, C. L. Zhang, H. C. Zhou, Z. H. Guo and L. Fang, *J. Mater. Chem. A*, 2020, **8**, 15891-15899.
20. J. Liu, D. Hua, Y. Zhang, S. Japip and T.-S. Chung, *Adv. Mater.*, 2018, **30**, 1705933.
21. D. Ren, Y. H. Li, S. P. Ren, T. Y. Liu and X. L. Wang, *J. Membr. Sci.*, 2020, **610**.